Eur. Phys. J. B **34**, 381–394 (2003)
DOI: 10.1140/epjb/e2003-00235-y

THE EUROPEAN PHYSICAL JOURNAL B

# Exchange bias like effect induced by domain walls in FeGd/FeSn bilayers

F. Canet[1], C. Bellouard[1,a], S. Mangin[1], C. Chatelain[1], C. Senet[1], R. Siebrecht[2], V. Leiner[2], and M. Piecuch[1]

[1] Laboratoire de Physique des Matériaux, Université Henri Poincaré Nancy 1, 54506 Vandoeuvre-les-Nancy, Cedex France
[2] Institut Laue Langevin, avenue des Martyrs, 38042 Grenoble Cedex 9, France

Received 20 February 2003
Published online 9 September 2003 – 

**Abstract.** A study of exchange bias phenomenon in ferrimagnetic /ferromagnetic FeGd/ FeSn bilayers is presented. The amorphous FeSn and FeGd alloys have been grown by co-evaporation. Specific growth conditions allow to induce an uniaxial anisotropy in both alloys in a parallel direction. After saturation of the bilayers under a positive field, the hysteresis loop of one of the layer is shifted towards a positive field $H_E$. The sign of the exchange bias field $H_E$ is shown to be due to the antiferromagnetic coupling between the net magnetizations of both alloys. The field $H_E$ is studied as a function of the thickness of each layer and of the temperature. Using ac-susceptibility measurements and polarized neutron reflectometry, it is shown that the reversal of magnetization of the bilayers is dominated by the presence of a domain wall at the interface. This exchange bias system is shown to act as a potential well for the magnetic domain wall. Within this assumption and thanks to a precise magnetic characterization of each alloy, the evolution of $H_E$ with the thickness of the layers is well reproduced using simple one-dimensional analytical models for the domain wall or a more elaborate numerical approach.

**PACS.** 75.60.Ch Domain walls and domain structure – 75.70.-i Magnetic properties of thin films, surfaces, and interfaces – 75.25.+z Spin arrangements in magnetically ordered materials (including neutron and spin-polarized electron studies, synchrotron-source X-ray scattering, etc.)

## 1 Introduction

### 1.1 Background

Despite the fact that the effect of exchange anisotropy has been discovered more than 40 years ago [1], this topic is still of great interest [2,3]. This effect results from interfacial interactions between a ferromagnetic (F) and an antiferromagnetic (AF). When both materials are cooled under an applied field across the Néel temperature $T_N$ of the AF, the hysteresis loop of the F is shifted along the field axis by a so called exchange bias field $H_E$. This loop shift is equivalent to an unidirectional anisotropy energy. In most systems, $H_E$ is negative (that is to say opposite to the cooling field) and weakly depends on the cooling field. However, positive values of $H_E$ have been found in $FeF_2$/Fe bilayers for high cooling fields [4]. $H_E$ vanishes for a so called blocking temperature $T_B$ which is closed to $T_N$ for most systems. The aim of the work performed on this topic is motivated by its applications in magnetoelectronic devices as well as the fundamental understanding of the origin of the effect which is still under heavy discussions.

The applications concern essentially two fields: the permanent magnet materials and the high density recording technology. Exchange anisotropy is actually used in giant magnetoresistive devices which consist of one metallic or insulating layer included between a free magnetic layer and a fixed one. The effect of exchange anisotropy is indeed used to control the magnetization reversal of the fixed layer. For this perspective, a high blocking temperature and a good temperature stability of the system are required. The control of the value of $H_E$ and the reduction of the demagnetizing field of the fixed magnetic layer (which may act on the soft one) are also of great interest.

Concerning the understanding of the origin of the effect, the following picture can be firstly proposed. When the system is field cooled, the AF spins at the interface between the two layers tend to align ferromagnetically with those of the F material (in the case of a ferromagnetic coupling). These AF spins exert a microscopic torque on the F spins which tend to keep their initial orientation [3]. Nevertheless, this naive picture cannot provide a quantitative evaluation of $H_E$. Anyway, as $H_E$ vanishes at $T_B \approx T_N$, the effect is due to the coupling with the AF material. For $H = H_E$, the change of Zeeman energy due to the reversal of the ferromagnetic material balances the change of interaction energy $\sigma$ between the two layers, $H_E$ ($t_F$) is then given by:

$$H_E(t_F) = \frac{\sigma}{2M_F t_F} \quad (1)$$

[a] e-mail: bellouard@lpm.u-nancy.fr

where $t_F$ and $M_F$ are respectively the thickness and the magnetization of the ferromagnetic material. $\sigma$ depends on the magnetic configuration at the interface. Several theoretical models have been developed to estimate $\sigma$. The most reliable models include the formation of domains in the AF or F layer [5,6], random exchange anisotropy [7], or 'spin-flop' perpendicular interfacial coupling [8]. The lack of an unified model arises from the difficulty to characterize and control the role of some structural and magnetic parameters as interface roughness and AF anisotropy.

### 1.2 Aim of the study

The aim of the present study is to propose a new system exhibiting an exchange bias like phenomenon with well-controlled magnetic characteristics which allow a simple quantitative interpretation of the exchange field. In conventional AF/F systems, the presence of the antiferromagnetic layer is found to have two big disadvantages for the understanding of the effect: first, as its net magnetization is equal to zero, it is difficult to obtain a clear picture of the magnetic configuration at the interface by any classical measurements. Secondly, the magnetic properties of those materials are usually poorly characterized because of the last remark. It was then decided to change the antiferromagnetic material by a ferrimagnetic alloy such as Rare Earth - Transition Metal (RE - TM) alloys.

Very specific exchange and anisotropy properties can be obtained with amorphous alloys of Rare-Earth (RE) and transition metals (TM). The exchange coupling of TM with light RE is ferromagnetic while it is antiferromagnetic with heavy RE. Very hard materials can be obtained in RE-TM alloys with Sm, Tb, or Nd. As a matter of fact, these materials play a crucial part in exchange spring magnets made of coupled hard -soft bilayers or multilayers [9–11]. On the other hand, very soft materials can be obtained with Gd. Moreover, an uniaxial anisotropy can be induced in these soft alloys with specific growth [12], or annealing conditions [13]. The use of RE-TM amorphous alloys allows then to avoid structural defects (observed in crystalline or polycrystalline samples), and to control both interfacial interactions and anisotropy properties.

A previous study, performed with GdFe/TbFe, has shown that it exhibits a negative exchange bias like phenomenon [14]. In this case, the bilayer is made of a soft material (GdFe) and a hard one (TbFe) with a ferromagnetic coupling. The system can be classified as a spring magnet. It has been shown that the reversal of the soft layer magnetization induces a magnetic domain wall (DW) at the interface [13–16]. In this case, the hard material acts as a potential barrier for the DW. In the case of antiferromagnetic coupling of two layers [13], the alignment of both magnetization with an applied field induces a domain wall at the interface between the layers.

The present study focuses on exchange coupled bilayer ferri /ferromagnetic $Fe_{60}Gd_{40}/Fe_{55}Sn_{45}$ which shows positive and negative exchange bias like effect. In this system, both layers are soft magnetic materials. $Fe_{60}Gd_{40}$ is ferrimagnetic with an antiferromagnetic coupling between Fe and Gd and a dominant contribution of Gd moments. The exchange coupling between the layers is dominated by the Fe-Fe interactions. As a result, in zero field, the configuration of the total magnetizations of the layers is antiferromagnetic. Moreover, an uniaxial anisotropy axis, necessary for a better understanding of the magnetization reversal, is induced during deposition in both alloys and in a parallel direction.

Preliminary results obtained by magnetization, susceptibility and magnetoresistance measurements on a $Fe_{60}Gd_{40}$ 1000 Å/$Fe_{55}Sn_{45}$ 800 Å bilayer have shown that this device exhibits an exchange bias like behavior: minor hysteresis loops corresponding to the reversal of one of the layers are shifted by a field $\pm H_E$ [17]. It has been shown that this reversal coincides with the creation or annihilation of a DW at the interface between the layers.

Here, we present further experimental results and also some quantitative interpretation of the exchange bias phenomenon. In-phase and out-of-phase susceptibility measurements have been performed to offer a distinction between reversible and irreversible processes in the magnetization reversal process. The use of polarized neutron reflectivity permits to observe the magnetic configuration in the bilayer as a function of an applied field. Thus, the position of the DW and its thickness can be determined. Finally, we have performed a systematic study of the magnetization reversal of $Fe_{60}Gd_{40}/Fe_{55}Sn_{45}$ bilayers as a function of the thickness of the layers. The influence of the temperature has also been investigated.

Quantitative interpretation of the observed results are presented. We have performed analytical and numerical calculations of the magnetic configuration within the bilayers. Firstly, considering the bilayer as a discontinuous linear chain of spins, we have analytically evaluated the energy of a DW at the interface between the layers as a function of its position. This calculation shows that the DW is confined in a potential well and is mainly located in one of the layers. Within this assumption, we propose a quantitative interpretation of the evolution of $H_E$ as a function of the thickness of the layers. Two simple analytical models for the DW, corresponding to a continuous or discontinuous chain of spins respectively, have been applied. The effect of the applied field on the DW has been simulated. The evolution of $H_E$ with temperature has been also accounted for. Also, to get a more precise picture of the magnetic configuration within the bilayer, numerical simulations have been performed which take into account the magnetic characteristics (magnetization, anisotropy, and exchange constant) of both alloys. These simulations provide the best fits of magnetization measurements and of the evolution of $H_E$ with the thickness of the layers.

### 1.3 Structure of the paper

This paper is divided as follows: first, some experimental details are clarified, then experimental results are presented. In this section, we first present the study of single layers which constitute the bilayer system. This permits to

obtain the magnetic characteristics of each layer. Typical magnetization loops of the $Fe_{60}Gd_{40}/Fe_{55}Sn_{45}$ system are then shown and qualitatively interpreted. The temperature and thickness dependence of $H_E$ is also shown. Further informations are obtained from in-phase and out-of-phase ac-susceptibility and polarized neutron reflectivity experiments. In the following section devoted to simulations, we firstly present analytical calculations which allow an evaluation of the energy of the bilayers as a function of the position of the DW. The evolution of $H_E$ with the thickness of the layers and some magnetization features are discussed in the frame of two one-dimensional analytical models for a 180° DW. More elaborate numerical simulations are then presented. The last section is devoted to discussion and conclusion.

## 2 Experimental details

$Fe_{60}Gd_{40}$ and $Fe_{55}Sn_{45}$ alloys were prepared by co-evaporation of the pure elements from three aligned crucibles in a high vacuum chamber. These alloys will be referred as FeGd and FeSn. The deposition rates were monitored by quartz oscillating systems, previously calibrated by optical methods. The substrates (glass or Si plates) were kept at 77 K in order to obtain amorphous alloys. The pressure was in the $10^{-8}$ torr range during the co-evaporation. The compositions of the alloys were checked by X-ray analysis and were found within the nominal values. The amorphicity of the alloys has been checked by transmission electron microscopy. The mean roughness of a 200 Å thick FeGd layer determined *ex situ* by atomic force microscopy is around 4 Å. The FeGd alloy, which is the most sensitive to oxidation, was always firstly deposited on the substrate. After preparation, the samples were kept at 77 K.

Magnetization measurements were performed with a superconducting quantum interference device magnetometer (SQUID). Susceptibility measurements were performed in a He-cryostat in the frequency range: 10–$10^4$ Hz. Both measurements were performed in the temperature range 5 K–350 K, and up to a static field of $10^4$ Oe.

The polarized neutron reflectivity experiment was carried out on the high flux reflectometer ADAM at the Institut Laue Langevin (Grenoble-France) [18]. The sample was cooled with a closed cycle cryostat to the lowest temperature (10 K). The magnetic field was provided by an electromagnet.

## 3 Experimental results

### 3.1 Magnetization results

#### 3.1.1 In-plane anisotropy

The aim of this part is to obtain the magnetic characteristics (exchange, anisotropy) of each alloy and to deduce the DW thickness and energy in both materials. These parameters will be used in the simulations of the experimental results obtained with the bilayers.

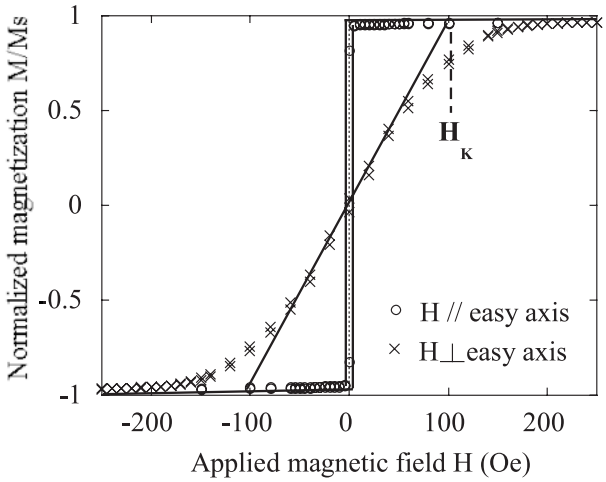


**Fig. 1.** Hysteresis loops of single 1000 Å thick FeGd layer measured at 5 K for an applied field parallel or perpendicular to the easy axis. $H_K$ is the anisotropy field of the Stoner and Wolfarth model.

Thin films of $Fe_{60}Gd_{40}$ are ferrimagnetic with a Curie temperature above 400 K [19]. We mention that the coupling between Fe and Gd is antiferromagnetic and that the net magnetization of the alloy is pointing along the moment of the gadolinium at all temperatures for this composition.

The presence of an uniaxial anisotropy in this alloy is clearly shown in Figure 1. It presents two hysteresis loops measured as a function of the applied magnetic field parallel ($H \parallel$) or perpendicular ($H \perp$) to the easy axis. The loop with $H \parallel$ is rectangular, whereas the loop with $H \perp$ shows vanishing remanence with almost no hysteresis, its evolution can be considered linear from $-H_K$ to $H_K$ where $H_K$ is the anisotropy field. The easy axis lies in the sample plane and is perpendicular to the vertical plane containing the sources [12]. Following the model of Stoner-Wohlfarth of uniform rotation [20], the anisotropy constant given by $K = \frac{M_S H_K}{2}$, where $M_S$ is the magnetization, can be deduced from the magnetization loops. From Figure 1, we evaluate an anisotropy constant equal to $7 \times 10^4$ erg/cm$^3$ with $M_S = 1000 \pm 100$ emu/cm$^3$ at $T = 5$ K. In a simple model of a DW treated as a linear continuous chain of spins, the domain wall thickness and energy in zero field are given by $\delta = \pi\sqrt{\frac{A}{K}}$ and $\sigma = 4\sqrt{AK}$ where $A$ is the effective exchange energy per unit length. Using the Mimura relation [21], which links together the exchange constant A of an alloy, the spin value, the interatomic distances and the exchange integrals, with $n_{\mathrm{Fe}} = 3$ and $n_{\mathrm{Gd}} = 3$ and the exchange integrals and spin values from reference [19]: $S_{\mathrm{Fe}} = 1$ and $S_{\mathrm{Gd}} = 7/2$, we find $A_{\mathrm{FeGd}} = 55 \times 10^{-8}$ erg/cm. The domain wall thickness and energy density are then evaluated to $\delta_{\mathrm{FeGd}} = 900$ Å and $\sigma_{\mathrm{FeGd}} = 0.7$ erg/cm$^2$ at $T = 5$ K for a 1000 Å thick

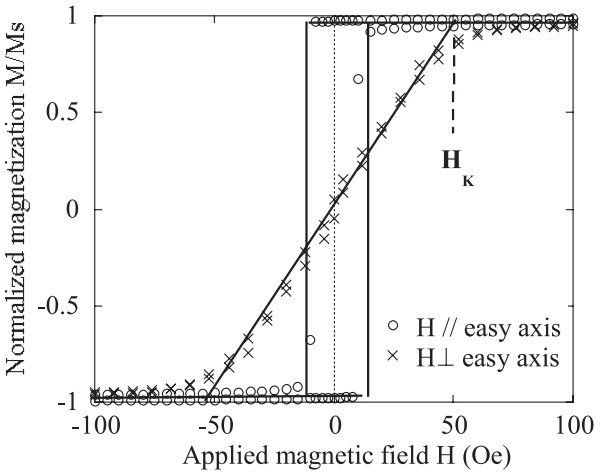


**Fig. 2.** Hysteresis loops of single 1000 Å thick FeSn layer measured at 5 K for an applied field parallel or perpendicular to the easy axis. $H_K$ is the anisotropy field of the Stoner and Wolfarth model.

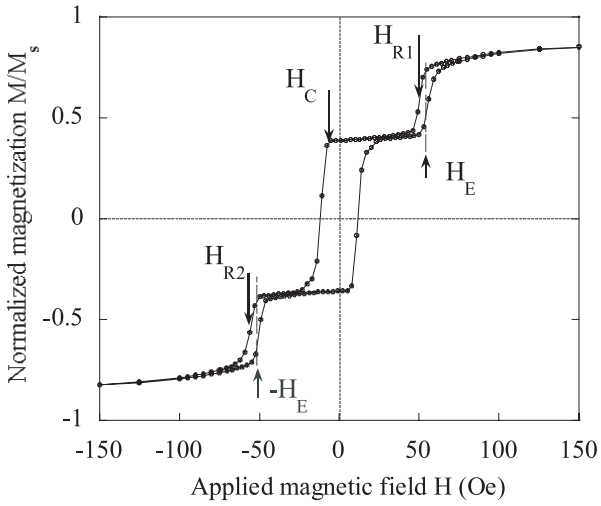


**Fig. 3.** Normalized magnetization *versus* field of a FeGd 1000 Å/FeSn 800 Å bilayer measured at 5 K.

layer. When the temperature is increased, both magnetization and anisotropy field decrease, resulting in an almost linear decrease of the anisotropy constant $K_{\mathrm{FeGd}}$ which is close to $0.6 \times 10^4$ erg/cm$^3$ at 300 K. When the thickness of the layer is decreased, the anisotropy field decreases whereas the magnetization stays unchanged. We evaluate an anisotropy constant $K_{\mathrm{FeGd}}$ of $2.8 \times 10^4$ erg/cm$^3$ for a thickness $t_{\mathrm{FeGd}}$ of 200 Å and then a zero field DW energy density $\sigma_{\mathrm{FeGd}}$ of 0.5 erg/cm$^2$ at $T = 5$ K.

Single layers of $Fe_{55}Sn_{45}$ are ferromagnetic with a Curie temperature close to 350 K in agreement with earlier studies [22]. Figure 2 shows that this alloy exhibits an uniaxial anisotropy. The anisotropy constant can be evaluated to $K_{\mathrm{FeSn}} = 1 \times 10^4$ erg/cm$^3$ with $M_s = 480 \pm 50$ emu/cm$^3$. From the mean field theory, we can deduce the exchange integral $j_{\mathrm{Fe-Fe}} = \frac{3k_B T_c}{2zxS(S+1)} = 6.6 \times 10^{-15}$ erg with the Curie temperature $T_c = 350$ K, the number of near-neighbors $z = 10$, the concentration $x = 0.55$ and the Fe spin equal to 1 [22]. The effective exchange energy per unit length of a domain wall $A_{\mathrm{FeSn}}$ can then be evaluated from the Mimura relation with $n_{\mathrm{Fe}} = 2$: $A_{\mathrm{FeSn}} = 15 \times 10^{-8}$ erg/cm. The domain wall thickness and energy density are evaluated to $\delta_{\mathrm{FeSn}} = 1300$ Å and $\sigma_{\mathrm{FeSn}} = 0.15$ erg/cm$^2$ for a 1000 Å thick layer at $T = 5$ K. When the temperature is increased, a decrease of both magnetization and anisotropy field is observed. This results in an almost linear decrease of the anisotropy constant which reaches $0.65 \times 10^4$ erg/cm$^3$ at $T = 300$ K. Unlike the $Fe_{60}Gd_{40}$ alloy, no thickness variation of the anisotropy field is observed in the range of thickness of 250 Å to 1500 Å.

In conclusion, we have clearly determined the magnetic properties of each alloy. They both exhibit an easy axis in the plane of the film and perpendicular to the direction made by the crucibles. As the three crucibles used for the evaporation of the bilayers are aligned, the anisotropy axis of the alloys are parallel. The estimated values of DW thickness and energy proposed above have to be considered only as an order of magnitude because of the crude assumptions made for the evaluation of $A$ (estimation of the number of nearest neighbors, of the exchange integrals). It provides nevertheless an useful material for comparison with values obtained from the study of the DW in the bilayers. We can from now on notice that the DW width is of the order of 1000 Å for both alloy and that the DW energy is much lower in the FeSn than in the FeGd alloy.

### 3.1.2 Characteristic magnetization loops of FeGd/FeSn bilayers

In this section, two typical magnetization loops obtained for two different bilayers are described.

Figure 3 shows the normalized magnetization (with respect to the magnetization measured for $H = 10$ kOe) of a FeGd 1000 Å/FeSn 800 Å bilayer at $T = 5$ K. The field has been applied along the common direction of the anisotropy axis of both layers. This loop exhibits three distinct steps. When the field is decreased from 10 kOe, the magnetization slowly decreases with decreasing field until a first drop of magnetization occurs for a positive field $H_{R1}$ followed by a plateau. When the field is reversed, two drops are observed for $H = H_C$ and $H = H_{R2}$. The magnetization then slowly reaches saturation as the amplitude of the field is further increased. When the field is swept back, symmetric loops are observed. These features can be interpreted as illustrated in Figure 4. In a high positive field ($H > 100$ Oe), the net moments of both layers tend to be aligned in the direction of the field. Because of the dominant ferromagnetic Fe-Fe exchange interaction which favors the alignment of the Fe moments of both layers, a domain wall of width $\delta$ spontaneously develops at the interface between the two layers: as the energy of a DW is lower in FeSn than in FeGd, we expect the DW to be located primarily in the FeSn alloy. Because of the uniaxial anisotropy of both alloys, this DW is a 180° Bloch wall with a modulation vector perpendicular to the film

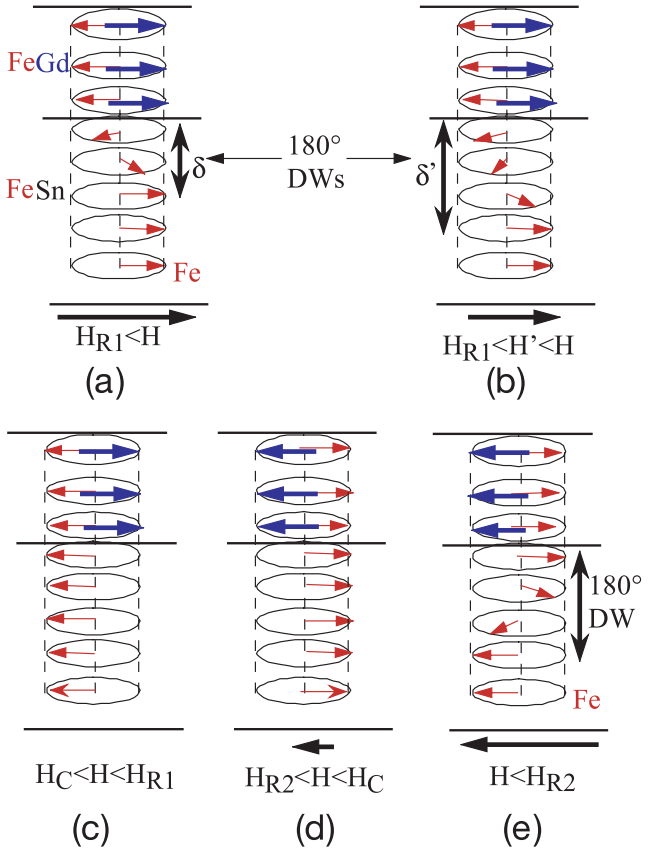


**Fig. 4.** Magnetic configurations of the bilayers for different stages of the magnetization loop.

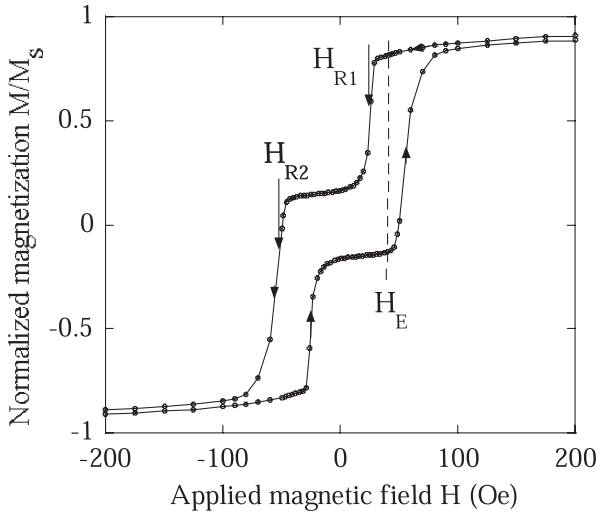


**Fig. 5.** Normalized magnetization versus field of a FeGd 600 Å/FeSn 1500 Å bilayer measured at 5 K.

plane. The magnetic configuration is illustrated in Figure 4a. When the field decreases, the magnetization decreases as this DW decompresses, *i.e.* further extends into the bilayer: $\delta' > \delta$ (Fig. 4b). For $H = H_{R1}$, the DW is annihilated with the reversal of the FeSn layer which has the lower total magnetic moment. Between $H_{R1}$ and $H_C$, the bilayer keeps its antiferromagnetic configuration without any DW (Fig. 4c) and the magnetization stays constant. From the magnetization of each alloy, it can be readily verified that the normalized magnetization of this plateau corresponds to the antiferromagnetic configuration. At $H = H_C$, the whole bilayer reverses (Fig. 4d). For $H \leq H_{R2}$, the FeSn reversal induces the creation of a DW in the bilayer which is then compressed when the amplitude of the field is increased (Fig. 4e).

When the field is swept back, the DW is decompressed. The variation of magnetization with decreasing and increasing field are nearly superimposed for $H < -70$ Oe as expected for compression and decompression stages which are reversible processes. The complete magnetization loop exhibits two minor loops associated to the reversal of the FeSn layer centered at $H = \pm H_E$. The width of these minor loops is due to the coercive field $H_C^{\mathrm{FeSn}}$ of the FeSn alloy. This is very similar to the exchange bias effect observed in AF/F bilayers where the magnetization loop is shifted toward positive or negative fields when the system is cooled under an applied field across the Néel temperature of the AF.

Figure 5 shows the normalized magnetization of a FeGd 600 Å/FeSn 1500 Å bilayer at $T = 5$ K. The main difference with the last case is that the magnetization per surface unit of the FeSn layer is higher that the one of the FeGd layer. Unlike the previous case, this magnetization loop exhibits only two steps of magnetization at $H = H_{R1}$ and $H = H_{R2}$. When a high positive field is applied, a 180° DW, as sketched in Figure 4a, spreads out in the FeSn layer as in the previous case. Also, as the field is decreased, this DW extends into the FeSn layer and the magnetization decreases (Fig. 4b). For $H = H_{R1}$, the DW is annihilated with the reversal of the FeGd layer which has the lower magnetic moment per surface unit in this bilayer. For $H_{R1} < H < H_{R2}$, the bilayer keeps an antiferromagnetic configuration as sketched in Figure 4d. For $H = H_{R2}$, the FeSn magnetization tends to be aligned with the field and a 180° DW is created in this layer (Fig. 4e).

### 3.1.3 Thickness and temperature dependence of $H_E$

A set of bilayers with different thickness ranging from 200 Å to 1500 Å for both alloys have been studied. All magnetization loops exhibit the same behavior as shown in Figures 3 or 5: when the field is decreased after saturation, a reversal of one layer is observed for a positive field $H_{R1}$, followed by a plateau of magnetization with a positive value of magnetization until the field is reversed. It has been clearly shown in the previous section that the layer which magnetization reverses in positive field is the one which has the lowest magnetization per surface unit. $H_E$ is then mainly a function of $\mu_{\mathrm{min}} = \min(t_{\mathrm{FeSn}} M_{\mathrm{FeSn}}, t_{\mathrm{FeGd}} M_{\mathrm{FeGd}})$ where $t_{\mathrm{FeSn}}$, $t_{\mathrm{FeGd}}$, $M_{\mathrm{FeSn}}$, $M_{\mathrm{FeGd}}$, are the thickness and saturation magnetization of

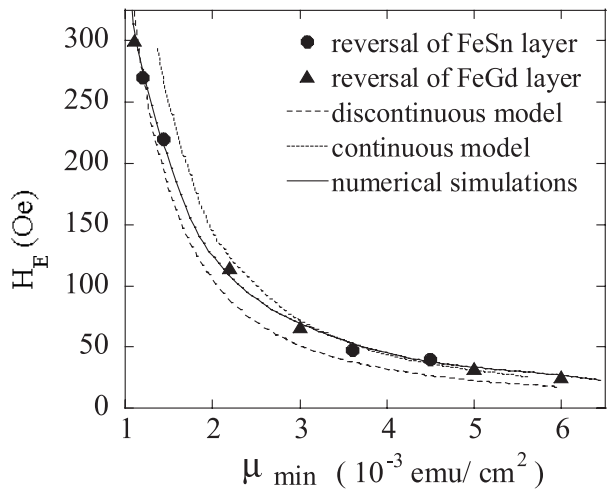


**Fig. 6.** Exchange field $H_E$ as a function of magnetization per surface unit of the reversing layer: $\mu_{min} = \min(t_{\mathrm{FeSn}} M_{\mathrm{FeSn}}, t_{\mathrm{FeGd}} M_{\mathrm{FeGd}})$, black circle: FeSn reversing layer, black triangle: FeGd reversing layer. The dotted and pecked lines are fits with the continuous and discontinuous model respectively. The straight line corresponds to numerical simulations.

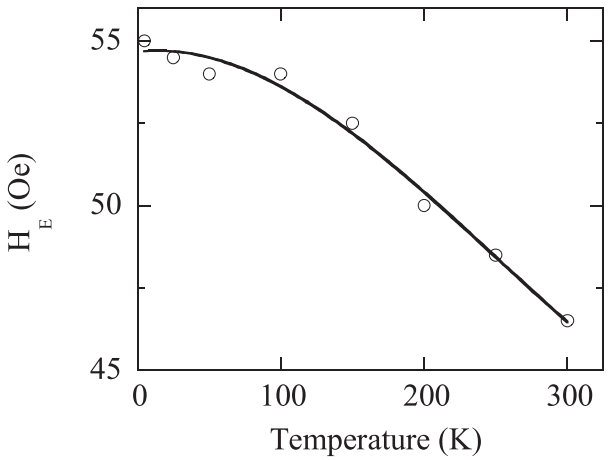


**Fig. 7.** Temperature dependence of $H_E$ for the FeGd 1000 Å/FeSn 800 Å bilayer. The straight line is a guide for the eye.

the FeSn and FeGd alloys respectively. Figure 6 shows the evolution of $H_E$ as a function of $\mu_{\min}$. A decrease of $H_E$ is observed as $\mu_{\min}$ increases.

Figure 7 shows the temperature dependence of $H_E$ for the FeGd 1000 Å/FeSn 800 Å bilayer. $H_E$ slightly decreases with increasing temperature from 5 K to 300 K. Both these evolutions will be interpreted in the section devoted to the analytical and numerical simulations.

To insure the simple model proposed for the magnetization reversal of a bilayer, we present below other experiments performed with ac-susceptibility measurements and polarized neutron reflectivity which are both sensitive to the presence of a DW.

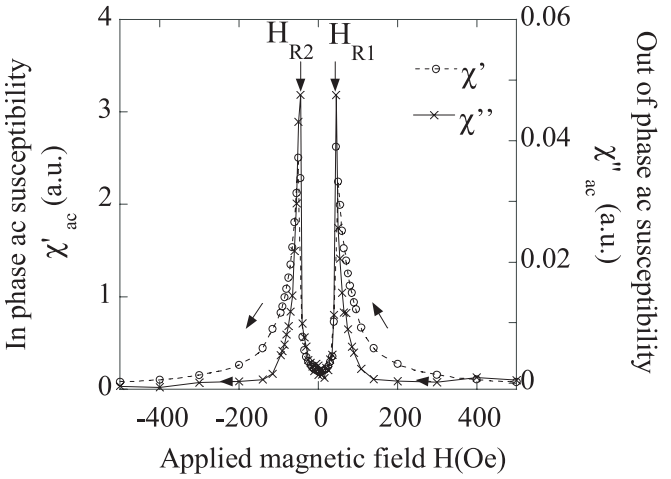


**Fig. 8.** In phase $\chi'$ and out of phase $\chi''$ ac susceptibility of a FeGd 1000 Å/FeSn 800 Å bilayer measured at 5 K with an applied field parallel to the easy axis.

### 3.2 Susceptibility results

In-phase $\chi'$ and out-of-phase $\chi''$ ac susceptibility have been measured with a 30 Hz frequency and a 2 Oe alternating field parallel both to the static field and to the easy axis. The signal is independent of the frequency in the range 10–$10^4$ Hz which are far from usual resonance frequencies of DW. $\chi'$ and $\chi''$ are plotted as a function of the static field in Figure 8 for the FeGd 1000 Å/FeSn 800 Å bilayer. The response to the excitation arises essentially from spins with a component perpendicular to the oscillating field. As those spins are present only in the DW, it makes the measurements very sensitive to the presence of DWs.

$\chi'$ corresponds to the linear response of the system and is sensitive to reversible processes. From Figure 8, we can observe that $\chi'$ increases as the width of the DW increases and that it drops to almost zero when the DW vanishes. It has been shown previously that $\chi'$ is proportional to $-\frac{\partial\delta(H)}{\partial H}$ [17], it then increases as the size of the DW increases.

$\chi''$ arises from irreversible processes. As a matter of fact, during the decompression or compression of the DW for $H > H_{R1}$ or $H < H_{R2}$, $\chi''$ is close to zero. $\chi''$ exhibits sharp peaks for $H$ close to $H_{R1}$ or $H_{R2}$, when the irreversible reversal of the FeSn layer occurs. Both $\chi'$ and $\chi''$ are close to zero when the configuration of the bilayer is antiferromagnetic between $H_{R1}$ and $H_{R2}$.

### 3.3 Polarized neutron reflectivity

Neutron reflectivity measurements were performed in order to investigate the orientation of magnetization for both alloys in the bilayer. The use of polarization analysis has allowed the measurement of the non spin flip reflected intensities $I^{++}$ and $I^{--}$, where the neutron keeps its polarization state before and after reflection. The measurements have been done with the FeGd 1000 Å/ FeSn 800 Å

bilayer and three applied fields: 15 Oe, 120 Oe and 2 kOe in order to observe the antiferromagnetic (AF) state and two DW states with different DW sizes (large DW (LDW) state: 120 Oe, small DW (SDW) state: 2 kOe).

For a better comparison of the evolution of the spectra with the field, the so-called $I^{++}$ and $I^{--}$ intensities have been chosen to refer to a polarization of the neutron parallel ($I^{++}$) and antiparallel ($I^{--}$) to the magnetization of the top of the bilayer. In the case of the DW state, the top of the FeSn layer is parallel to the field, in the case of the antiferromagnetic state, the top layer is indeed antiparallel to the applied field. The measured reflected intensities are plotted in Figures 9a, b, c as a function of the momentum transfer $q$ of the neutron perpendicular to the surface. The critical angle of the total reflection is proportional to $\sqrt{b+p}$ when the polarization of the neutron is parallel to the magnetization of the top layer and to $\sqrt{b-p}$ when it is antiparallel, $b$ is the nuclear scattering length, $p$ is the magnetic scattering length proportional to the magnetization. The total reflection occurs at the same $q$ value for the three spectra in each figure: this corroborates that the top of the FeSn layer is always parallel or antiparallel to the field. Nevertheless, the three spectra corresponding to the three magnetic fields are clearly different. One can notice that the oscillations of the AF state (15 Oe) and the LDW state (120 Oe) are almost out phase: for instance, for $q = 0.025$ Å$^{-1}$, $I^{++}$ is minimum for $H = 120$ Oe whereas it is maximum for the same q value and $H = 15$ Oe.

Simulated reflected intensities, calculated with a program based on the formalism described in reference [23], are also plotted in Figure 9. Three sets of parameters must be distinguished: (i) real and imaginary nuclear scattering length density, magnetic scattering length density, these parameters, which can be firstly evaluated from tables, bibliography and magnetic measurements, are characteristic of the alloys; (ii) thickness and roughness of the layers, these parameters concern the structure of the bilayer which can be evaluated with measurements of the deposited thickness during evaporation and with *ex situ* atomic force microscopy, (iii) finally, parameters concerning the magnetic configuration of the layers. Parameters (i) and (ii) have been firstly evaluated, they have then been changed around their nominal values to get a reasonable agreement between experimental data and simulation for the AF spectra (Fig. 9a). Characteristics of the bilayer deduced from the parameters used for simulations and corresponding value deduced from other measurements are reported in Table 1. The real and imaginary part of the density of nuclear scattering lengths correspond to an atomic density of $3.3 \times 10^{22}$ at /cm$^3$ for FeGd alloy and $5.4 \times 10^{22}$ at/cm$^3$ for FeSn. This last value is in agreement with previous measurements [24] ($5.4 \times 10^{22}$ at/cm$^3$). The magnetic scattering lengths correspond to magnetizations of 530 emu/cm$^3$ and 870 emu/cm$^3$ for the FeSn and FeGd alloys respectively, which agree with magnetization measurements (Tab. 1). The thickness of the layers used in the simulations: 990 Å for FeGd and 790 Å for FeSn are in good agreement with the evaluation made during evaporation. The roughness of the layers: 10 Å for the FeSn layer and 8 Å for FeGd correspond also to a reasonable value for amorphous alloys, we recall that a roughness of 4 Å has been measured with a 200 Å thick FeGd layer (from atomic force microscopy).

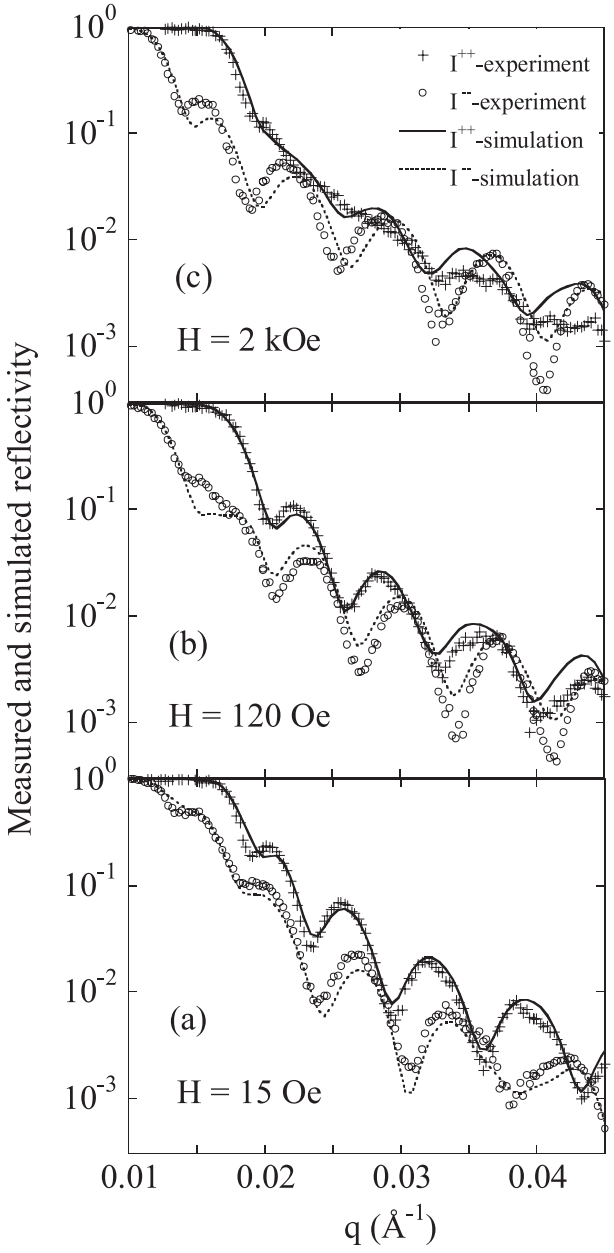


**Fig. 9.** Measured and calculated polarized neutron reflected intensity $I^{++}$ and $I^{--}$ as a function of $q$ for the FeGd 1000 Å/FeSn 800 Å bilayer for different applied fields: (a): $H = 15$ Oe, (b): $H = 120$ Oe, (c):$H = 2$ kOe.

Once these parameters have been chosen, they were kept unchanged for the simulations of the DW states. Considering firstly the spectra for $H = 120$ Oe, the simulated intensities plotted in Figure 9b are obtained with a 180° DW enterely located in the FeSn layer. The FeSn layer has been divided into 20 sublayers, the magnetic scattering length density of each layer is proportional to

**Table 1.** Characteristics of the bilayer deduced from the parameters used for the simulation of the neutron reflectivity spectra: layers thickness and roughness, magnetization and atomic density of the alloys, the nominal layer thickness deduced from measurements during evaporation and the magnetization measured on individual layers are also reported.

| | Thickness used for simulation (Å) | Nominal thickness (Å) | Atomic density used for simulation (at / cm$^3$) | Roughness used for simulation (Å) | Magnetization deduced from simulation (emu/cm$^3$) | Measured Magnetization (emu/cm$^3$) |
|---|---|---|---|---|---|---|
| FeGd | 990 | 1000 | $3.3 \times 10^{22}$ | 8 | 870 | $1000 \pm 100$ |
| FeSn | 790 | 800 | $5.4 \times 10^{22}$ | 10 | 530 | $480 \pm 50$ |

$\cos\theta$ where $\theta$ is the angle between the field and the magnetization of the sublayer. We have assumed that $\theta = 0$ for the top layer and that $\theta = \pi$ at the interface with the FeGd. The evolution of $\cos\theta$ with the distance of the sublayer from the interface is plotted in Figure 10. A DW width of about 300 Å is obtained. Within the assumption that the DW is spread in both layers, for instance, if we assumed that a 90° DW is present in both layers, the calculated intensities totally deviate from the experimental ones. The spectra for $H = 2$ kOe have been firstly simulated with a ferromagnetic configuration (no DW in the bilayer), in that case, large discrepancies with the experimental data are observed, specially for the $I^{--}$ reflection. The simulations plotted in Figure 9c have been obtained with a DW totaly included in the FeSn layer with a 80 Å width (Fig. 10). As it will be shown by numerical simulation, a small part of the DW could enters for this field in the FeGd layer. Assuming that the DW is spread in both layer with a 30° DW in the FeGd layer and a 150° DW the FeSn layer, the simulated spectra fit the experimental data almost as in Figure 9c. Neutron reflectivity allows then to confirm the presence of a DW for $H = 2$ kOe but do not allow to state if a small part enters or not the FeGd layer. In the same way, because of the poor agreement between simulations and experimental spectra for both DW states, a change of 20% of the DW width does not clearly modify the quality of the fitting between simulation and experiment.

As a conclusion, these measurements corroborate the presence of a DW at the interface between the layers which is mainly included in the FeSn layer, and also the decrease of the DW width with increasing field.

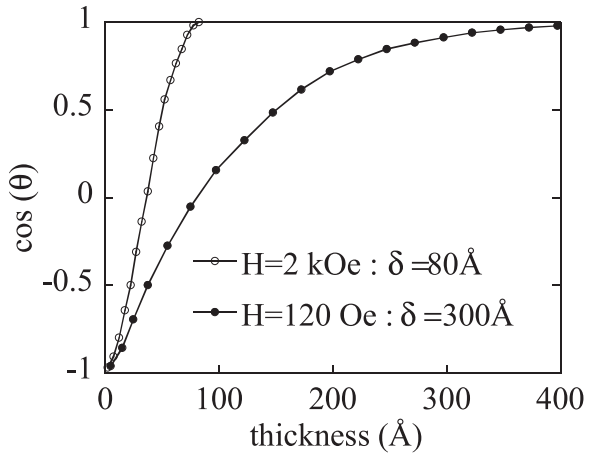


**Fig. 10.** Profile of the DW used for the simulations of the neutrons spectra. $\delta$ is the evaluated width of the DW.

## 4 Simulations of magnetic reversal in FeGd/FeSn bilayers

Magnetization, ac-susceptibility and polarized neutrons reflectivity measurements clearly show the formation of a DW in FeSn/FeGd bilayers at the interface between the layers. Moreover, the neutron experiment has shown that this DW is preferentially located in the FeSn layer. This DW can be compressed by an applied field. The exchange bias field is found to be the field at which the DW is annihilated or created. $H_E$ slightly depends on the temperature but clearly depends on the thickness of the reversing layer. In the present section, we will show that the bilayer system can be modeled as a potential well for the DW. The magnetic profile as a function of the applied field, and the temperature and thickness dependence of the exchange field, will be studied using analytical and numerical models.

If the coercivity of the reversing layer near $H_E$ is neglected, *i.e.*, no structural defects pin the DW, one can assume that the system always adopts the magnetic configuration which minimizes its energy. We firstly present a simple calculation of the energy of the bilayer, submitted to an applied field, as a function of the position of the DW. This permits to localize the DW and to see the effect of the field. We propose a quantitative analysis of magnetization results with one-dimensional models for the DW that permit analytical calculations. The DW is supposed to be entirely confined in the FeSn layer. In the models used, the DW is treated both as a discontinuous or as a continuous linear chain of spins. Values for domain wall thickness and energy is derived from both models. These expressions permit an analysis of the DW compression

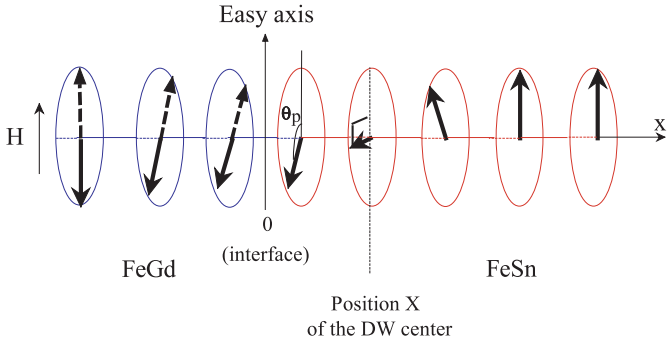


**Fig. 11.** Schematic view of the bilayer with a DW spread in both layers. The full arrows represent the Fe moments and the dotted one represent the Gd moments.

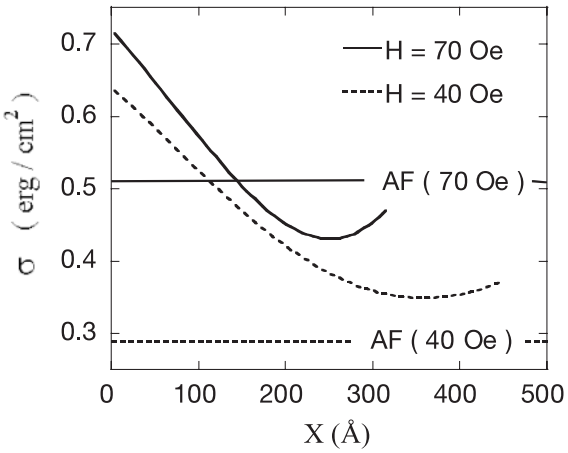


**Fig. 12.** Energy of a DW as a function of its distance from the interface in the FeSn layer for two applied fields: 40 Oe and 70 Oe. The straight lines correspond to the energy of the AF state of a FeGd 1000 Å/FeSn 800 Åbilayer for the same fields.

stage in the magnetization loop, of the evolution of $H_E$ as a function of the layers thickness and also as a function of temperature. Finally, we present results obtained from numerical simulations which take into account the magnetic characteristics of both alloys and provide the magnetic profile of the total bilayer.

### 4.1 A Basic equation: balance sheet of energy

The bilayer is considered as a chain of spin divided in two parts corresponding to the FeSn and FeGd layers (see Fig. 11). When a field is applied, it is assumed that a DW is present between the two layers. The aim of the present calculation is to determine with simple assumptions the magnetic configuration which minimizes the energy of the whole chain, it is then modeled as a potential well.

The DW is located with the abscissa $X$ of the moment with an angle $\theta_i = (\vec{M}_i, \vec{H}) = \frac{\pi}{2}$ which represents the 'center' of the DW. $X = 0$ corresponds to a 180° DW centered at the interface, which can be divided in two 90° DWs included in the FeSn and in the FeGd layer respectively. $X$ is positive (respectively negative) when the moment for which $\theta = \frac{\pi}{2}$ belongs to the FeSn layer (respectively to the FeGd layer). The energy of the DW with respect to the saturated state has been calculated as a function of $X$. In fact, as it will be shown below, the minimum of the energy of the bilayer is always found for $X > 0$, that is why the case $X < 0$ has not then been investigated. The moments in the FeSn layer are assumed to rotate from 0 at the top of the layer to an angle $\theta_p$ near the interface. In the assumption of a discontinuous linear chain of spins, the $\theta_i$ angles vary linearly with the position in the FeSn layer. Because of the AF coupling between FeSn and FeGd, the moments in the FeGd layer rotate from 0 far away from the interface to $\pi - \theta_p$ at the interface with the FeSn layer. The energy of the 180° DW is given by $\sigma(X) = \sigma_{\mathrm{FeSn}} + \sigma_{\mathrm{FeGd}}$, where $\sigma_{\mathrm{FeSn}}$ denotes the energy of the $(\theta_p)$ DW in the FeSn layer, and $\sigma_{\mathrm{FeGd}}$ the energy of the $(\pi - \theta_p)$DW in the FeGd layer. The calculation of the characteristics of a $(\theta_p)$DW for a discontinuous chain of spins is detailed in the appendix.

When $\theta_p > \frac{\pi}{2}$, the 'center' $X$ of the DW in the FeSn alloy is given by

$$X = \theta_p \left(1 - \frac{\pi}{2\theta_p}\right) \times \sqrt{\frac{2A_{\mathrm{FeSn}}}{K_{\mathrm{FeSn}}\left(1 - \frac{\sin 2\theta_p}{2\theta_p}\right) + 2M_{\mathrm{FeSn}}H\left(1 - \frac{\sin\theta_p}{\theta_p}\right)}}.$$

The contribution of the FeSn and FeGd alloys to the DW energy are then given by:

$$\sigma_{\mathrm{FeSn}} = \theta_p \sqrt{2A_{\mathrm{FeSn}}\left(K_{\mathrm{FeSn}}\left(1 - \frac{\sin 2\theta_p}{2\theta_p}\right) + 2M_{\mathrm{FeSn}}H\left(1 - \frac{\sin\theta_p}{\theta_p}\right)\right)}$$

and

$$\sigma_{\mathrm{FeGd}} = (\pi - \theta_p)\left(2A_{\mathrm{FeGd}}\left(K_{\mathrm{FeGd}}\left(1 + \frac{\sin 2\theta_p}{2(\pi - \theta_p)}\right) + 2M_{\mathrm{FeGd}}H\left(1 - \frac{\sin\theta_p}{\pi - \theta_p}\right)\right)\right)^{1/2}$$

$\sigma(X)$ is plotted in Figure 12 for two applied fields. This calculation has been done with parameters (exchange constants, anisotropy constants and saturation magnetization values ) evaluated in the previous section. Both curves exhibit the shape of a potential well. The maximum $X$ value corresponds to $\theta_p = \pi$ when the DW is entirely located in the FeSn layer, $X$ is then given by the half width of the DW. For all fields, the minimum of $\sigma(X)$ is located in the FeSn layer. It corresponds to a $\theta_p$ value of 161° and 157° for $H = 40$ Oe and 70 Oe respectively: the main part of the DW is included in the FeSn layer. The minimum of $\sigma(X)$ shifts towards the interface as the field increases, this is the signature of the compression

of the DW. The energy of the antiferromagnetic state called $AF(H)$ is also shown in Figure 12 in the case of the FeGd 1000 Å/FeSn 800 Å bilayer. This energy is calculated with respect to the saturated state and is given by $AF(H) = 2M_{\mathrm{FeSn}}t_{\mathrm{FeSn}}H$ where $M_{\mathrm{FeSn}}$ and $t_{\mathrm{FeSn}}$ denote saturation magnetization and thickness of the FeSn layer, respectively. For $H = 40$ Oe $< H_E$, the minimum energy state is reached for an antiferromagnetic configuration whereas for $H = 70$ Oe $> H_E$, the energetically most favorable state is described by the formation of a DW. This is in agreement with the experimental results. The DW is then located in a potential well unless the energy of the AF configuration is lower than the energy of the DW state. In that case, the system drops to the AF state. For $H = H_E$, the energy of the DW state must be equal to the one of the AF state. For any bilayers, the following equation can then be written:

$$2\mu_{\min} H_E = \sigma(H_E) \tag{2}$$

where $\mu_{min} = \min(t_{\mathrm{FeSn}}M_{\mathrm{FeSn}}, t_{\mathrm{FeGd}}M_{\mathrm{FeGd}})$ is the magnetic moment per surface unit of the layer which reverses at $H_E$. Note that this expression is equivalent to (1).

## 4.2 DW simulated with one dimensional analytical models

In the following, equation (2) mentioned above will be used to evaluate $H_E$. Our goal is to obtain a simple model which fits the evolution of $H_E$ with the thickness of the layers and with temperature (Figs. 6 and 7). To get an analytical expression for $\sigma$ $(H_E)$, some simplifying assumptions will be made: the DW will be supposed to be located entirely within the FeSn layer and will be considered, firstly as a discontinuous and, in a second approach, as a continuous linear chain of spins.

### 4.2.1 Models

(a) *Discontinuous linear chain of spins*

The thickness and energy of a $(\theta_p)$ DW for a discontinuous chain of spins is presented in the appendix. From these expressions, the thickness and energy of a 180° DW can be simply deduced with $\theta_p = \pi$:

$$\delta(H) = \pi\sqrt{\frac{2A}{K+2MH}} = \pi\sqrt{\frac{2}{1+4h}\,\frac{A}{K}} \text{ with } h = \frac{H}{H_K} \tag{3}$$

$$\sigma(H) = \pi\sqrt{2A(2MH+K)} = \pi\sqrt{2AK(1+4h)}. \tag{4}$$

(b) *Continuous linear chain of spins*

We consider a semi-infinite linear chain of spins, where $\theta(z)$ is the angle between the field applied along the easy direction, $H$, and the spin at position $z$. The excess energy due to the presence of a 180° domain wall is given by:

$$E = \int_{-\infty}^{0}\left[A\left(\frac{\partial\theta}{\partial z}\right)^2 + MH(1-\cos\theta(z)) + K\sin^2\theta(z)\right]dz. \tag{5}$$

The minimization of this expression with the boundary conditions $\theta(-\infty) = 0$ and $\theta(0) = \pi$ gives $\theta(z) = 2\arctan\left[\sqrt{\frac{h+1}{h}}\,\frac{1}{\mathrm{sh}(z/\xi(h))}\right]$ where $h = \frac{H}{H_K}$ and $\xi(h) = \sqrt{\frac{A}{(1+h)K}}$. This model is more realistic than the previous one as it provides an asymmetric DW profile: *i.e.* the rotation of the spins increases as $z$ approaches 0 or $\theta$ approaches $\pi$.

The domain wall thickness can be evaluated by $\delta(h) = \pi\xi(h)$ and the domain wall energy is given by

$$\sigma(h) = 4\sqrt{AK}\left[h\,\mathrm{Ln}\left(1+\sqrt{1+h}\right) - \frac{h}{2}\mathrm{Ln}(h) + \sqrt{1+h}\right]. \tag{6}$$

### 4.2.2 Simulations of experimental results

(a) *Domain wall compression*

For $H > H_{R1}$, the magnetization loop shows an increase of magnetization with applied field corresponding to a compression of the domain wall. If this domain wall is located in the FeSn layer, the magnetization of the bilayer is given by:

$$\frac{1}{t_{\mathrm{FeGd}}+t_{\mathrm{FeSn}}}(M_{\mathrm{FeGd}}t_{\mathrm{FeGd}} + M_{\mathrm{FeSn}}(t_{\mathrm{FeSn}} - \delta(H))) \tag{7}$$

Figure 13 shows a fit of magnetization of the FeGd 1000 Å/FeSn 800 Å bilayer for $H > H_{R1}$ with this expression where $\delta(H)$ is given by the discontinuous model (3). The anisotropy constant has been fixed to the value obtained for the FeSn alloy with single layers measurements. The fitted value of magnetization are 965 and 445 emu/cm$^3$ for FeGd and FeSn alloys respectively in agreement with magnetization measurements (which yielded $1000 \pm 100$ emu/cm$^3$ and $480 \pm 50$ emu/cm$^3$). The fit also provides a value of the exchange constant $A = 17 \times 10^{-8}$ erg/cm close to the evaluation made with mean field theory for the FeSn alloy ($A = 15 \times 10^{-8}$ erg/cm).

From equation (7), we can evaluate the size of the DW for the magnetic fields studied during the neutron experiment. We obtain $\delta = 400$ Å and 80 Å for $H = 120$ Oe and 2 kOe respectively. These values are close to the size deduced from the DW profile of figure 10 (300 Å and 80 Å).

(b) *Dependence of $H_E$ on the thickness of the layers*

The fits of $H_E$ with equation (2) and using expressions (4) and (6) for the energy of the domain wall are plotted in Figure 6. For these fits, the magnetization $M$ and

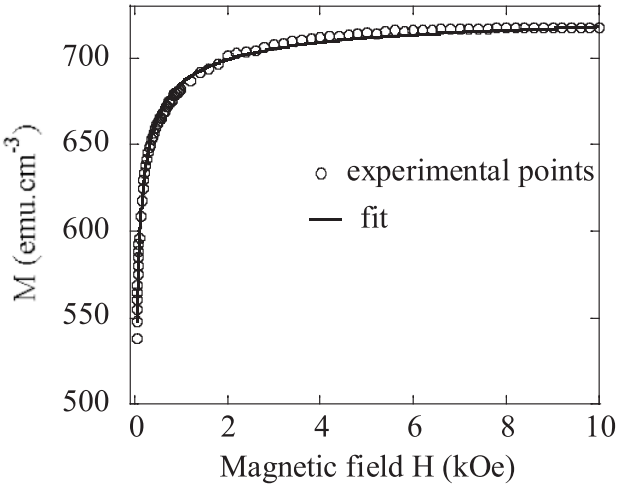


**Fig. 13.** Magnetization of the FeGd 1000/FeSn 800 bilayer *versus* applied field (open circles) fitted by the discontinuous model (straight line).

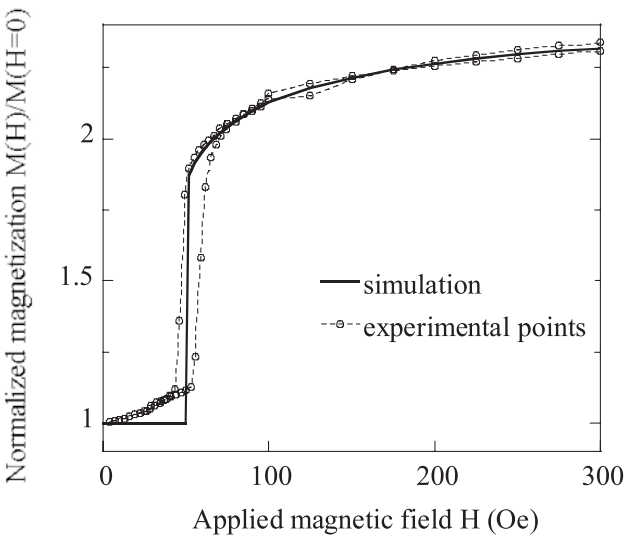


**Fig. 14.** Measured and simulated magnetization loop of the FeGd 1000 Å/FeSn 800 Å bilayer. The simulation has been made with numerical simulations.

anisotropy constant $K$ have been fixed to the value obtained from measurements on single layers, only the value of the exchange constant $A_{\mathrm{FeSn}}$ has been varied. It is observed that at low fields the discontinuous model and at higher fields the model of a continuous spin chain are less appropriate to properly reproduce the experimental results. Nevertheless, the fits provide values for the effective exchange constant of $8\times10^{-8}$ erg/cm for the discontinuous model and $16\times10^{-8}$ erg/cm for the continuous that are close to the evaluation made for the FeSn alloy from mean field theory ($15\times10^{-8}$ erg/cm). This insures the assumption of the localization of the DW in the FeSn layer, as the exchange constant in the FeGd alloys is much higher. We recall that the more realistic model is the continuous one as it allows an asymmetric profile of the DW in an applied field.

(c) *Temperature dependence of $H_E$*

Figure 7 shows the temperature dependence of $H_E$ for the FeGd 1000 Å/FeSn 800 Å bilayer as obtained from magnetization measurements. $H_E$ slightly decreases with increasing temperature from 5 K to 300 K. This temperature dependence is related to the temperature dependence of magnetization, exchange constant and anisotropy of both alloys. In the frame of the more simple model, using equations (2) and (4) and considering that the exchange constant is proportional to the square of magnetization, it is obvious to deduce that $\left[\frac{H_E(T_1)}{H_E(T_2)}\right]^2 = \frac{2M_{\mathrm{FeSn}}(T_1)H_E(T_1)+K_{\mathrm{FeSn}}(T_1)}{2M_{\mathrm{FeSn}}(T_2)H_E(T_2)+K_{\mathrm{FeSn}}(T_2)}$. Considering the temperature dependence of $M_{\mathrm{FeSn}}$ and $K_{\mathrm{FeSn}}$ obtained from measurements on single layers, with $H_E = 55$ Oe at 5 K, we can calculate $H_E = 38$ Oe at 300 K which is close to the measured value ($43 \pm 3$ Oe, derived from magnetization measurements). This crude model permits to recover the slight decrease of $H_E$ with increasing temperature.

### 4.3 DW simulated with numerical simulations

To get a more precise picture of the magnetization profile in the bilayers, we have performed numerical simulations which take into account the magnetic characteristics of both alloys (magnetization, anisotropy and exchange constants). The magnetic configuration is supposed to be uniform within the plane of the bilayer and to vary only along the direction perpendicular to the sample surface. We can then treat the bilayers as a discrete chain of $n$ spins, its magnetic configuration is given by the $n$ angles $\theta_i$ between each moment $\vec{u}_i$ and the applied field $H$. The exchange energy between $\vec{u}_i$ and $\vec{u}_{i+1}$ is proportional to $2A_id_i$ where $A_i$ denotes the exchange constant and $d_i$ the distance between neighboring moments or planes of the material. Each moment is subjected to an uniaxial anisotropy $k_i$ parallel to the applied field. The angles $\theta_i$ are obtained by minimization of the total energy $E_{tot}$:

$$E_{tot} = \sum_{i=1}^{n} -\mu_i H\cos(\theta_i) + k_i\sin^2(\theta_i) - 2A_id_i\cos(\theta_i-\theta_{i+1}) \tag{8}$$

with $A_n = 0$. The first two terms and the last term represent the one and two-sites interactions, respectively. The dipolar energy has been neglected as the moments lie in the plane of the layers.

This minimization of equation (8) with respect to the n angles $\theta_i$ has been done with a method introduced by Derrida and Vannimenus [25], which allows an exact calculation of the $\theta_i$ angles which take $p$ discrete values between 0 and $2\pi$ . This method has been previously used for the study of interfaces in random media at zero temperature. The calculation takes advantage of the fact that there are only nearest-neighbor interactions in the energy.

The simulated magnetization loop $M(H) = \sum_i \mu_i \cos\theta_i$ is plotted in Figure 14 with the experimental data. The calculated magnetic configuration with this method always gives the true state if unique and is insensitive to the presence of metastable states. The later explains the absence of hysteresis in the magnetization curve in Figure 14. The calculations have been done with $p = 4000$. Values for the magnetic moment $\mu_i$ and anisotropy $k_i$ per site have been deduced from single layers measurements assuming the same atomic density as for the bilayer used in the neutron simulations. The distances between planes have been evaluated to 2.65 Å and to 3 Å in the FeSn and FeGd alloys respectively. Only the exchange constants inside the alloys $A_{\mathrm{FeSn}}$ and $A_{\mathrm{FeGd}}$ and between the layers $A_{\mathrm{FeSn/FeGd}}$ have been adjusted in order to obtain the best agreement with the experimental results. The decrease of magnetization due to a decompression of the DW and the step of magnetization at $H = H_E$ are well reproduced by the simulation. The exchange parameters inside the alloys are $A_{\mathrm{FeSn}} = 23 \times 10^{-8}$ erg/cm, $A_{\mathrm{FeGd}} = 72 \times 10^{-8}$ erg/cm which are close to the evaluation made with mean field theory ($A_{\mathrm{FeSn}} = 15 \times 10^{-8}$ erg/cm, $A_{\mathrm{FeGd}} = 55 \times 10^{-8}$ erg/cm). The antiferromagnetic exchange coupling has been determined to $A_{\mathrm{FeSn/FeGd}} = -56 \times 10^{-8}$ erg/cm. The obtained DW profile $\cos\theta_i$ is plotted in Figure 15 for several fields: 80 Oe, 250 Oe and 2 kOe. The profile is asymmetric even for 80 Oe. The DW is always mainly confined in the FeSn layer. Nevertheless, the rotation of the moments inside the FeGd layer increases when the field increases: *i.e.* the DW increasingly "enters" the FeGd layer. Keeping the exchange constants fixed, we have performed simulations for other thicknesses of the FeSn layer. These simulations have been made with the same set of parameters (all parameters are then fixed), we have neglected the dependence of the anisotropy constant of the FeGd alloy with the thickness of the layer (which is not significant as the domain wall is mainly confined in the FeSn layer). The field of the step of magnetization $H_E$ is plotted in Figure 6: the experimental variation of $H_E$ is perfectly reproduced by the simulations.

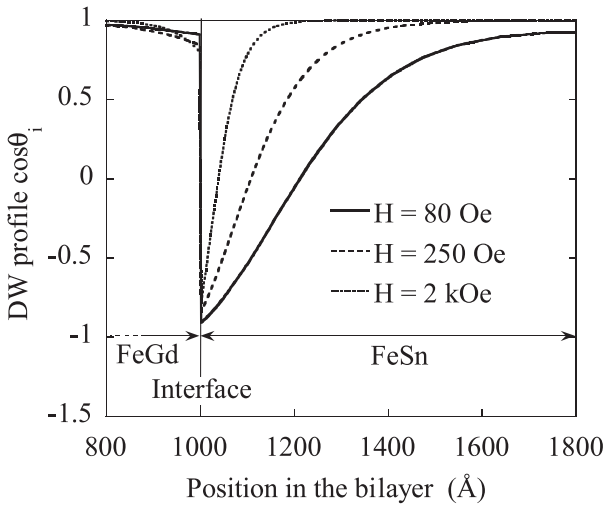


**Fig. 15.** Magnetization profile of the FeGd 1000 Å/FeSn 800 Å bilayer deduced from numerical simulations. This profile is given by cos $\theta$ where $\theta$ is the angle between each moment and the applied field.

## 5 Discussion and conclusion

Antiferromagnetic exchange coupled bilayers FeSn / FeGd have been prepared by co-evaporation. This technique has allowed to induce in-situ a well-defined uniaxial anisotropy in each layer. Magnetic properties of both alloys have been well quantitatively characterized. In this system, since the net magnetization of the ferrimagnetic material is parallel to the moment held by the rare earth, and the interface coupling is dominated by the ferromagnetic Fe-Fe exchange interaction, it results in an antiferromagnetic coupling at the interface between the two layers.

For all FeSn and FeGd thickness (between 200 Å and 1500 Å), we observed exchange bias phenomenon, that is to say, the shift of the hysteresis loop of one of the layer towards a field $H_E$. The layer which magnetization reverses at $H_E$ is the one which has the lower magnetization per surface unit. The field $H_E$ is found to depend strongly on the layer thickness and slightly on temperature. The use of magnetization susceptibility and polarized neutron reflectometry permits to draw the following explanation.

When a large field is applied along the easy axis of both layers, the two magnetizations tend to be aligned along the field. But because the coupling between the magnetizations is antiferromagnetic, a DW is created at the interface. As the amplitude of the field is decreased, the DW tends to grow (DW decompression). However when the DW energy is larger than the Zeeman energy needed to reverse one of the layer, an antiparallel alignment of the two layers is favorable. As a consequence, the magnetization of one of the layer rotates at a positive field $H_E$ and leads to the annihilation of the DW. The exchange bias phenomena in that case is then dominated by the presence of an interfacial DW. Polarized neutron reflectometry has clearly shown the presence of the DW and is in agreement with the assumption of the localization of the DW in the softer FeSn alloy.

In order to give credit to the above interpretation and allow a quantitative understanding, a simple model for which the whole bilayer is considered as a discontinuous chain of spin has been developed. The system is supposed to keep its minimum energy state when the position of the DW is varied. This shows that the system acts as a potential well which traps the interface DW. The center of the DW is always located in the FeSn layer. When the applied field is increased, the well gets deeper and the minimum energy is localized closer to the interface. This is consistent with the observed compression of the DW under an applied field.

For $H = H_E$, the change of Zeeman energy of the reversing layer balances the energy of the DW. With the assumption of the location of the DW to be within the FeSn layer, the evolution of $H_E$, as a function of the net moment of the reversing layer, is well described within the frame of two analytical models for the DW, treated as a continuous and as a discontinuous linear chain of spins. The model of a continuous spin chain was found to be more appropriate and properly yields an asymmetric profile for the DW. The variation of $H_E$ with temperature is also accounted for. Moreover, using a numerical calculation which takes into account the characteristics of both alloys, the best fit of the dependence of $H_E$ with the moment of the reversing layer is obtained and the magnetization measurements well reproduced.

In conclusion we have grown a new type of system which exhibits exchange bias phenomenon: (ferrimagnetic GdFe/ ferromagnetic FeSn). It has been shown that the magnetic properties of the FeSn/FeGd system are well characterized and controlled and it offers a preferential system for the investigation of DW via susceptibility and neutron reflectivity measurements. It then constitutes a model for the understanding of the role of DW in less known systems.

It may be compared to conventional exchange bias system (AF/F):

Concerning fundamental understanding of the magnetization reversal processes, it is clear that in the studied Ferri/Ferro the phenomenon is dominated by creation, compression- decompression of interface DW. Note that this explanation is very similar to the one given by Mauri in the case of AF/F bilayers [5]. In our case, thanks to the amorphous structure which avoids the presence of structural defects, no formation of domains and lateral DW have to be taken into account. The main difference between the two systems is that the ferrimagnetic alloy is not fully compensated as the antiferromagnetic alloy.

For the applications, ferri/ferro system based on TM compounds, might be an alternative for the design of magnetoresistive systems. Indeed, it was shown that the amplitude of the exchange bias could be easily controlled and that this field was thermally stable. Also, because of the antiferromagnetic coupling at the interface, such bilayer can be tailored to display a small magnetic moment. Thus the dipolar coupling between the free and the fixed layer, in for example a spin valve or tunneling junction device, can be minimized. Finally, as Curie temperatures for ferrimagnetic material can be larger than usual Néel temperature in AF material, we can expect these devices to have a higher limiting temperature.

## Appendix

The $(\theta_p)$ DW is considered as a discontinuous linear chain of $n+1$ spins $i$ making an angle $\theta_i$ with respect to the applied field; $\theta_0 = 0$, $\theta_n = \theta_p$, and $\theta_i = i\frac{\theta_p}{n}$. The width of the wall is given by $\delta_{\theta_p} = nd$ where $d$ is the distance between neighboring spins.

The chain is submitted to an uniaxial anisotropy with energy constant per unit volume $K$ and to an applied field $H$ parallel to the easy axis. The effective exchange energy per unit length of the chain is $A$, and the magnetization of the material $M$. The excess of exchange-, anisotropy- and Zeeman-energy per surface unit due to the presence of the domain wall, with respect to the saturated state, is given by:

$$\begin{aligned}\sigma_{\theta_p} &= 2\frac{A}{d}\left(n - \sum_{i=0}^{n-1}\cos(\theta_{i+1}-\theta_i)\right) \\ &\quad + d\,K\sum_{i=0}^{n}\sin^2\theta_i + d\,M\,H\left(n - \sum_{i=0}^{n}\cos\theta_i\right) \\ &\approx \frac{A}{n\,d}\theta_p^2 + \frac{ndK}{2}\left(1 - \frac{\sin 2\theta_p}{2\theta_p}\right) + ndMH\left(1 - \frac{\sin\theta_p}{\theta_p}\right) \\ &\qquad\qquad \text{for } n \gg 1.\end{aligned}$$

The minimization of this expression as a function of $n$ provides the DW width:

$$\delta_{\theta_p} = n\,d = \theta_p\sqrt{\frac{A}{\frac{K}{2}\left(1 - \frac{\sin 2\theta_p}{2\theta_p}\right) + M\,H\left(1 - \frac{\sin\theta_p}{\theta_p}\right)}}.$$

If $\theta_p > \frac{\pi}{2}$, the center $X$ of the DW, defined as the distance between the spin $n$ and the spin with $\theta_i = \frac{\pi}{2}$, is given by:

$$\begin{aligned}X &= n\,d\left(1 - \frac{\pi}{2\theta_p}\right) = \theta_p\left(1 - \frac{\pi}{2\theta_p}\right) \\ &\quad \times \sqrt{\frac{A}{\frac{K}{2}\left(1 - \frac{\sin 2\theta_p}{2\theta_p}\right) + M\,H\left(1 - \frac{\sin\theta_p}{\theta_p}\right)}}.\end{aligned}$$

The energy of the $\theta_p$ DW is:

$$\sigma_{\theta_p} = \theta_p\sqrt{2A\left[K\left(1 - \frac{\sin 2\theta_p}{2\theta_p}\right) + 2M\,H\left(1 - \frac{\sin\theta_p}{\theta_p}\right)\right]}.$$

## References


1. W.H. Meiklejohn, C.P. Bean, Phys. Rev. **102**, 1413 (1956); W.H. Meiklejohn, C.P. Bean, Phys. Rev. **105**, 904 (1957)
2. A.E. Berkowitz, K. Takano, J. Magn. Magn. Mater. **200**, 552 (1999)
3. J. Nogues, I.K. Schuller, J. Magn. Magn. Mater. **192**, 203 (1999)
4. J. Nogues, C. Leighton, I.K. Schuller, Phys. Rev. B **61**, 1315 (2000)
5. D. Mauri, H.C. Siegmann, P.S. Bagus, E. Kay, J. Appl. Phys. **62**, 3047 (1987)
6. M. Kiwi, J. Majia-Lopez, R.D. Portugal, R. Ramirez, Appl. Phys. Lett. **75**, 3995 (1999)
7. A.P. Malozemoff, Phys. Rev. B **35**, 3679, (1987); A.P. Malozemoff, Phys. Rev. B **37**, 7673 (1988)

8. N.C. Koon, Phys. Rev. Lett. **78**, 4865 (1997)
9. J.S. Jiang, E.E. Fullerton, M. Grimsditch, C.H. Sowers, J. Pearson, S.D. Bader, Phil. Mag. B **80**, 247, (2000)
10. E.E. Fullerton, J.S. Jiang, S.D. Bader, J. Magn. Magn. Mater. **200**, 392 (1999)
11. M.E. Shrabes, E.E. Fullerton, D.T. Margulies, IEEE Trans. Magn. **37**, 1432 (2001)
12. S. Mangin, C. Bellouard, G. Marchal, B. Barbara, J. Magn. Magn. Mater. **165**, 161 (1997)
13. B. Dieny, D. Givord, J.M.B. Ndjaka, J. Magn. Magn. Mater. **93**, 503 (1991); B. Dieny, D. Givord, J.M.B. Ndjaka., J.M. Alameda, J. Appl. Phys. **67**, 5677 (1990); S. Wuchner, J.C. Toussaint, J. Voiron, Phys. Rev. B **55**, 11576 (1997)
14. S. Mangin, G. Marchal, B. Barbara, Phys. Rev. Lett. **82**, 4336 (1999); S. Mangin, G. Marchal, C. Bellouard, W. Wernsdorfer, B. Barbara, Phys. Rev. B **58**, 2748 (1998)
15. K. Mibu, T. Nagahama, T. Shinjo, T. Ono, Phys. Rev. B **58**, 6442 (1998)
16. M. Sawicki, G.J. Bowden, P.A.J. de Groot, B.D. Rainford, J.-M.L. Beaujour, R.C.C. Ward, M.R. Wells, Phys. Rev. B **62**, 5817 (2000)
17. F. Canet, S. Mangin, C. Bellouard, M. Piecuch, Euro. Phys. Lett. **52**, 594 (2000)
18. R. Siebrecht, A. Schreyer, U. English, U. Pietsch, H. Zabel, Physica B **241**, 169 (1998)
19. P.Hansen, C. Clausen, G. Much, M. Rosenkranz, K. Witter, J. Appl. Phys. **66**, 756 (1989)
20. E.C. Stoner, E.P. Wohlfarth, Philos. Trans. London. Ser. A **240**, 599 (1948)
21. Y. Mimura, N. Imamura, T. Kobayashi, A. Okada, Y. Kushiro, J. Appl. Phys. **49**, 1208 (1978)
22. B. Rodmacq, M. Piecuch, C. Janot, G. Marchal, P. Mangin, Phys. Rev. B **21**, 1911 (1980)
23. S.J. Blundell, J.A.C. Bland, Phys. Rev. B **46**, 1339 (1992)
24. J.F. Geny, G. Marchal, P. Mangin, C. Janot, M. Piecuch, Phys. Rev. B **25**, 7449 (1982)
25. B. Derrida, J. Vannimenus, Phys. Rev. B **27**, 4401 (1983)